IFAC Journal of Systems and Control 36 (2026) 100414

Contents lists available at ScienceDirect

IFAC Journal of Systems and Control

journal homepage: www.elsevier.com/locate/ifacsc

Full length article

Artificial pancreas under stable pulsatile Model Predictive Control: Including the physical activity effect☆

Nicola Licini [a,*], Beatrice Sonzogni [a], Pablo Abuin [a,b], Fabio Previdi [a], Alejandro H. González [b], Antonio Ferramosca [a]

[a] Department of Management, Information and Production Engineering, University of Bergamo, 24044 Dalmine, Bergamo, Italy
[b] Institute of Technological Development for the Chemical Industry (INTEC), CONICET-Universidad Nacional del Litoral, Güemes 3450, (3000), Santa Fe, Argentina

ARTICLE INFO

Article history:
Received 30 April 2025
Received in revised form 17 March 2026
Accepted 7 April 2026
Available online 16 April 2026

Keywords:
Type 1 diabetes
Artificial pancreas
Physical activity
Model Predictive Control

ABSTRACT

Type 1 diabetes management presents significant challenges due to the complex interplay between insulin delivery, carbohydrate intake, and physical activity. This paper introduces an enhanced artificial pancreas system based on stable pulsatile Zone Model Predictive Control (pZMPC) that explicitly addresses the metabolic effects of physical activity. The proposed approach integrates (i) a novel dynamical model that captures physical activity's impact on glucose–insulin dynamics, (ii) the incorporation of a non-standard insulin-on-board constraint to prevent hypoglycemia, and (iii) the implementation of an asymmetric cost function that penalizes hypoglycemia more severely than hyperglycemia. The control strategy was evaluated using in silico trials with a virtual population of ten patients under various realistic scenarios, including meal and exercise announcement errors and circadian variations in insulin sensitivity.

© 2026 The Author(s). Published by Elsevier Ltd. This is an open access article under the CC BY license (http://creativecommons.org/licenses/by/4.0/).

1. Introduction

Type 1 Diabetes Mellitus (T1DM) is a chronic autoimmune disease that leads to the destruction of pancreatic β-cells, responsible for producing endogenous insulin. The absence of insulin impairs glucose uptake by cells, resulting in elevated Blood Glucose (BG) levels and long-term complications (Katsarou et al., 2017). To maintain glucose levels within the *euglycemic* range (70–180 [mg/dL]), Functional Insulin Therapy (FIT) has been introduced as a substitute for endogenous insulin regulation. FIT consists of continuous basal insulin infusion during fasting and postprandial/correction boluses to mitigate (transitory) hyperglycemic episodes (Howorka, 2012). However, the effectiveness of FIT is limited by uncertainties, such as meal estimation errors, variations in insulin sensitivity, and the impact of external factors like stress and physical activity (PA), among others. Advancements in Continuous Glucose Monitoring (CGM) sensors and Continuous Subcutaneous Insulin Infusion (CSII) pumps have led to the development of the Artificial Pancreas (AP), an automated system for BG regulation. At the core of the AP is a control algorithm that computes insulin delivery based on CGM readings. Among the various control strategies, Model Predictive Control (MPC) has emerged as one of the most promising approaches (Bondia et al., 2018; Incremona et al., 2018). MPC determines the optimal insulin dose by solving a constrained finite-horizon optimization problem, leveraging a mathematical model to predict BG dynamics and minimize deviations from target values. Despite the effectiveness of AP systems based on MPC algorithms, numerous challenges remain, with PA being one of the most significant. Many individuals with T1DM avoid exercise due to its unpredictable effects on BG regulation. For instance, aerobic PA increases insulin sensitivity and glucose consumption, often leading to hypoglycemia (Dalla Man et al., 2009). However, exercise also provides substantial health benefits for T1DM patients, including improved cardiovascular fitness and metabolic health (American Diabetes Association, 2003). To mitigate exercise-related risks, various guidelines have been proposed (Colberg et al., 2016). Still glucose control during exercise remains a challenge due to the interplay of exercise type, duration, intensity, meal timing, and pre-exercise glucose levels. From a control-oriented perspective, PA acts as a disturbance similar to meal ingestion, prompting increased glucose consumption based on intensity and duration (Mansell et al., 2017; Roy, 2007). A recent research (Romeres et al., 2021) has identified two primary effects of PA on BG levels: (i) an insulin-independent effect that directly increases glucose clearance, and (ii) an insulin-dependent effect that alters insulin sensitivity.

☆ This article is part of a Special issue entitled: 'BMS 2024' published in IFAC Journal of Systems and Control.

* Corresponding author.
E-mail address: nicola.licini@unibg.it (N. Licini).

https://doi.org/10.1016/j.ifacsc.2026.100414
2468-6018/© 2026 The Author(s). Published by Elsevier Ltd. This is an open access article under the CC BY license (http://creativecommons.org/licenses/by/4.0/).

1.1. General physical activity management

The general approach to manage physical activity in T1DM involves planning and anticipation of the event. Typically, to counteract the effect of exercise and to avoid consequent hypoglycemic episodes, basal and, if necessary, postprandial bolus insulin doses are reduced shortly before the exercise event (American Diabetes Association, 2003; Riddell et al., 2017). In a closed-loop insulin delivery system, such as the MPC-based AP, this means that over the prediction horizon, the controller is aware of the upcoming activity, allowing insulin delivery to be adjusted, thus reducing the risk of hypo- and hyperglycemic episodes during and after the exercise routine (feedforward control).

However, relying completely on a planned approach to exercise management has significant limitations. Real life is unpredictable, as are patients' daily routines and activities; expecting them to plan every workout or exercise session meticulously may be impractical or unrealistic. In addition, unforeseen circumstances associated with PA (i.e. a sudden rush or jump), can have a significant impact on blood glucose levels. This unpredictability highlights the need for more adaptive and flexible coping strategies that go beyond planned activities.

There is no doubt that the ultimate goal is to manage physical activity without any intervention or announcement from the patient; however, this outcome is still far from being achieved.

1.2. Contributions

According to the aforementioned discussion, the main novelty of this work is the extension of the glucose–insulin regulation model to incorporate the effects of PA insulin-independent glucose clearance, by extending the framework proposed in Abuin et al. (2024). The control strategy for individual T1DM patients employs a pulsatile Zone MPC (pZMPC) Abuin et al. (2024), Gondhalekar et al. (2018), aiming to maintain BG within the safe range by delivering insulin exclusively in pulse form, covering both basal and bolus requirements. The performance of the proposed algorithm is evaluated under two physical activity scenarios: (i) Programmed PA, where the exercise session is known to the controller in advance over the prediction horizon (i.e., pre-announced by the patient); and (ii) Non-Programmed PA, where PA is announced only at the onset of the exercise session. Finally, to assess the controller's robustness, an analysis have been done incorporating circadian variations in insulin sensitivity and event-announcement errors.

1.3. Paper organization

The remainder of this paper is organized as follows: Section 2 details the methodology, presenting the extended compartmental model that incorporates physical activity effects, and describing the constraints applied in the control formulation. Section 3 introduces the pZMPC framework, including the asymmetric cost function design and the implementation of insulin-on-board constraint. Sections 4 and 5 describe the in silico experimental protocol and present the work's results. Finally, Section 6 concludes the paper with a summary of contributions and directions for future research.

2. Methods

This section presents the model proposed in the work to handle PA effect together with details on controllability and the constraints that will be used in the pZMPC depicted in Section 3.

2.1. Prediction model

The following extension of the Ruan physiological long-term model (Ruan et al., 2017), considering the effect of the physical activity is used to describe the glucose–insulin subsystem:

$$\begin{aligned} \dot{x}(t) &= Ax(t) + B_u u(t) + B_r r(t) + B_p p(t) + E \\ y(t) &= Cx(t) \end{aligned} \tag{1}$$

where $x(t) = [x_1(t), x_2(t), x_3(t), x_4(t), x_5(t), x_6(t), x_7(t)]'$, are the system states. In particular, $x_1(t)$ represents the blood glucose concentration [mg/dL], selected as the measurable output of the system (i.e., the glycemia to be controlled, $y(t)$); $x_2(t)$ the insulin delivery rate in plasma [U/min]; $x_3(t)$ the insulin delivery rate in the subcutaneous compartment [U/min]; $x_4(t)$ the rate of carbohydrate absorption from the gut [g/min]; $x_5(t)$ the glucose delivery rate from the stomach [g/min]; and $x_6(t)$ and $x_7(t)$ the insulin-independent PA subsystem. This latter is described by the following linear dynamical model, whose order is selected to reflect the dynamics of the physical activity disturbance:

$$\frac{dx_6(t)}{dt} = -\frac{1}{\theta_7}x_6(t) + \frac{1}{\theta_7}x_7(t) \tag{2}$$

$$\frac{dx_7(t)}{dt} = -\frac{1}{\theta_7}x_7(t) + \frac{1}{\theta_7}p(t) \tag{3}$$

being $G_{PA}(t) = \theta_6 x_6(t)$ the net effect of PA on BG system. This term represents the net effect of increased muscle glucose uptake and reduced hepatic glucose production during PA, independently of insulin action (Romeres et al., 2021). Finally, $u(t)$ is the insulin infusion [U/min], $r(t)$ is the rate of the carbohydrate (CHO) intake in each unit of time [g/min] and $p(t)$ is the PA intensity level (expressed as a percentage of the maximum rate of oxygen consumption, $\%VO_2^{max}$). The model matrices are given by:

$$A = \begin{pmatrix} -\theta_1 & -\theta_2 & 0 & \theta_3 & 0 & -\theta_6 & 0 \\ 0 & -\frac{1}{\theta_4} & \frac{1}{\theta_4} & 0 & 0 & 0 & 0 \\ 0 & 0 & -\frac{1}{\theta_4} & 0 & 0 & 0 & 0 \\ 0 & 0 & 0 & -\frac{1}{\theta_5} & \frac{1}{\theta_5} & 0 & 0 \\ 0 & 0 & 0 & 0 & -\frac{1}{\theta_5} & 0 & 0 \\ 0 & 0 & 0 & 0 & 0 & -\frac{1}{\theta_7} & \frac{1}{\theta_7} \\ 0 & 0 & 0 & 0 & 0 & 0 & -\frac{1}{\theta_7} \end{pmatrix},$$

$$B_u = \begin{pmatrix} 0 \\ 0 \\ \frac{1}{\theta_4} \\ 0 \\ 0 \\ 0 \\ 0 \end{pmatrix} \quad B_r = \begin{pmatrix} 0 \\ 0 \\ 0 \\ 0 \\ \frac{1}{\theta_5} \\ 0 \\ 0 \end{pmatrix}, \quad B_p = \begin{pmatrix} 0 \\ 0 \\ 0 \\ 0 \\ 0 \\ 0 \\ \frac{1}{\theta_7} \end{pmatrix}, \quad E = \begin{pmatrix} \theta_0 \\ 0 \\ 0 \\ 0 \\ 0 \\ 0 \\ 0 \end{pmatrix},$$

$$C = \begin{pmatrix} 1 & 0 & 0 & 0 & 0 & 0 & 0 \end{pmatrix}.$$

where θ_1 is the glucose effectiveness [min^{-1}] or glucose self-regulation effect to promote its own metabolism (i.e. stimulating glucose uptake by peripheral tissues and suppressing hepatic glucose release), θ_2 is the insulin sensitivity [mg/(dL·U)], θ_3 is the carbohydrate raising factor [mg/(dL·g)], being the rate of glucose appearance in plasma $Ra = \theta_3 x_4$ [mg/(dL·min)], θ_6 the rate of blood glucose utilization due to PA level [mg/dL], and θ_0 the endogenous glucose production at basal levels EGP_b ($\theta_0 = \theta_1 G_b + \theta_2 U_b$, being G_b and U_b the glucose and insulin rate at basal levels) [mg/(dL·min)]. Finally, the input absorption kinetics are expressed by θ_4, θ_5 and θ_7 [min], which represent, respectively, the time-to-maximum effective insulin concentration, the time-of-maximum appearance rate of glucose in the gut, and the time constant related to the PA subsystem. Fig. 1 resumes the model structure.

Table 1
Estimated parameters of 10 in-silico adult patients.

Patient	001	002	003	004	005	006	007	008	009	010
θ_0 [mg/dL]	1.7674	2.2987	1.5972	1.529	0.936	2.0073	2.2833	1.4514	2.0225	1.4373
θ_1 [min^{-1}]	0.0044	0.007	0.0043	0.0039	0.0027	0.0062	0.004	0.0051	0.0049	0.0047
θ_2 [mg/(dL·U)]	59.3372	62.5857	41.2591	66.6716	37.1395	39.4356	84.1097	41.0676	90.6396	42.7168
θ_3 [mg/(dL·g)]	3.0974	2.784	2.8372	3.384	2.7605	4.3881	4.6368	4.6739	4.5867	3.1022
θ_4 [min]	56.0072	40.0138	52.206	59.508	45.516	52.5146	47.5143	50.0135	50.513	50.5091
θ_5 [min]	29.1351	19.3239	32.8563	32.6981	27.5781	26.9012	28.1041	32.31	27.4438	28.1452
θ_6 [mg/dL]	1.5573	1.4404	1.2914	1.6856	1.5856	1.3678	2.0136	2.0324	1.7418	1.1299
θ_7 [min]	5.4441	4.9463	3.3443	7.8859	11.1741	8.1516	3.9166	18.0647	1.8449	0.6605

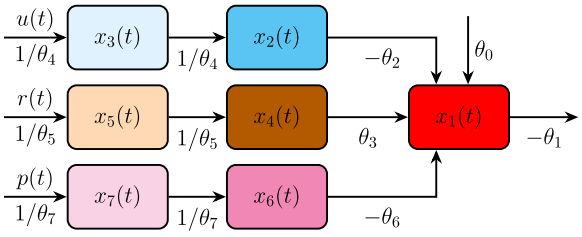

Fig. 1. Graphical representation of the extended Ruan physiological long-term model, incorporating the effect of physical activity (PA). The diagram illustrates the glucose–insulin subsystem, where $x_1(t)$ represents blood glucose concentration, influenced by insulin delivery $u(t)$, carbohydrate intake $r(t)$, and PA level $p(t)$. The model includes compartments for insulin absorption ($x_2(t), x_3(t)$), carbohydrate digestion ($x_4(t), x_5(t)$), and insulin-independent glucose uptake due to PA ($x_6(t), x_7(t)$). The basal endogenous glucose production (θ_0) contributes to glucose dynamics, while parameterized transfer rates ($\theta_1, \dots, \theta_7$) determine the interactions among compartments.

Personalization of the general glucose–insulin model (1) for each patient, has been carried out by following the parameter estimation routine based on regularized least-squares (RLS) outlined by Licini et al. (2024). For a cohort of 10 in-silico patients from the UVA/Padova Simulator (Group, 2016), the proposed model achieved a validation GoF with a median [25th, 75th] of 55.29 [52.66, 63.45]. Table 1 presents the resulting parameter configurations. Compared with Abuin et al. (2020), the parameter θ_2 (insulin sensitivity) was overestimated by an average of 10.8%. This discrepancy is likely due to the UVA/Padova simulator accounting for the insulin-dependent component of PA, which is not fully captured by the Ruan model (Ruan et al., 2017).

Remark 1. From model (1), FIT standard tools can be derived. Parameter θ_2 gives the correction factor (or insulin sensitivity factor) CF [mg/(dL · U)], θ_3 gives the raise factor (or carbohydrate factor) RF [mg/(dL · g)]. It follows the carbohydrate-to-insulin ratio (or the number of carbohydrates covered by 1 unit of insulin) $CR = CF/RF = \theta_2/\theta_3$ [g/U]. Finally, the insulin basal rate is defined as $U_b = (\theta_0 - \theta_1 G_b)/\theta_2$ [U/min].

Remark 2. Insulin on Board (IOB), i.e. the amount of insulin remaining in the body from previous insulin boluses, can be derived from the two compartments of the model (1), that are devoted to describe the insulin subsystem (Abuin et al., 2020). Indeed, $IOB(t) := \int_0^t (u(\tau) - x_2(\tau))d\tau = \int_0^t \theta_4(\dot{x}_2(\tau) + \dot{x}_3(\tau))d\tau = \theta_4(x_2(t) + x_3(t))$ where $x_i(0) = 0$ with $i = \{2, 3\}$.

Remark 3. The input (control action) $u(t)$ can be expressed as the superposition of its basal and bolus (or postprandial, pp) infusions, U_b and u_{pp}, such that:

$$u(t) := U_b + u_{pp}(t). \tag{4}$$

As a result, the controller is in charge of the total insulin infusion, increasing the system controllability in case of external disturbances (i.e. meals and physical activity). According to this superposition, the same reasoning holds for the state variables $x_i(t) = x_{i,b}(t) + x_{i,pp}(t)$, with $i = \{1, 2, 3\}$ and for the insulin on board $IOB(t) = IOB_b + IOB_{pp}(t)$, as presented in Abuin et al. (2024).

2.2. Time-varying input and state constraints

Constraints on both input and states have been assumed for system (1), such that $u \in \mathcal{U}$, with $\mathcal{U} = \{u \in \mathbb{R}_{\geq 0} | u \leq U_{max}\}$, with $U_{max} = 15$ [U/min] (i.e. maximum erogable insulin dose from insulin pumps) (MiniMed, 2018). Moreover, $x \in \mathcal{X}(t)$, where $\mathcal{X}(t)$ is assumed to vary throughout the day to meet the requirements of postprandial periods:

$$\begin{aligned}\mathcal{X}(t) := \{x \in \mathbb{R}^7_{\geq 0} | & G_{hypo} \leq x_1(t) \leq G_{hyper}, \\ & \theta_4(x_2(t) + x_3(t)) \leq \overline{IOB}(t)\}\end{aligned} \tag{5}$$

where x_1 is bounded by $G_{hypo} = 54$ and $G_{hyper} = 300$ [mg/dL], to prevent severe hypo- and severe hyperglycemia, while $\overline{IOB}(t) = \overline{IOB}_b + \overline{IOB}_{pp}(t; t_0, \hat{CHO}_0)$ is an upper bound for the insulin on board. Here, $\hat{CHO}_0$ is the meal announcement of carbohydrate content [g] at time $t = t_0$. Thus, IOB_b and IOB_{pp} denote the basal (equilibrium, constant) and postprandial (meal-size-dependent) values of the constraint, defining the admissible insulin injection throughout the day. This follows the non-standard IOB constraint proposed in Abuin et al. (2024), which depends on the meal-bolus size $U_0 = \hat{CHO}_0/CR$ and a fixed interval ΔT_{IOB} (e.g. $\Delta T_{IOB} = 60$ [min] for all patients). Finally, notice that $\mathcal{X}(t)$ is unbounded from above for meal and physical activity related states, i.e. x_j $j \in \{4, 5, 6, 7\}$, which is consistent with the fact that these components are uncontrollable.

As part of the system/problem description, a target set $\mathcal{Y}_{Tar}$ is defined as $\mathcal{Y}_{Tar} \doteq \{y \in \mathbb{R} : G_{min} \leq y \leq G_{max}\}$, where G_{min} and G_{max} are, respectively, 90 [mg/dL] and 120 [mg/dL]. Note the difference between a constraint set $\mathcal{X}$ and a target set $\mathcal{Y}_{Tar}$, in the sense that the system may be outside the latter during the transient regime, while it must be inside the former at any time: $\mathcal{X}$ is associated to the domain of validity of the model, while $\mathcal{Y}_{Tar}$ is the target where the prediction is led to.

3. Pulsatile MPC formulation

This section presents the pulsatile Zone MPC (pZMPC) introduced in Abuin et al. (2024), considering both a non-standard IOB constraint and an asymmetric cost function, designed to penalize hypoglycemic excursions more than hyperglycemic ones. The proposed MPC uses state predictions based on the discrete-time pulsatile representation of the model (1) (see Appendix). Its primary objective is to maintain blood glucose (BG) within a safety zone $\mathcal{Y}^{Tar}$, while satisfying input and state constraints along the control trajectory. The states are estimated by an "Output Disturbance Observer" (ODO), which provides an offset-free estimation when the plant-model mismatch is in the form of an impulse, a step, or a ramp (as detailed in Abuin et al., 2020). Although pZMPC is also designed for unannounced input cases, this work focuses solely on the announced (or partially announced)

disturbances scenario. In particular, the estimated carbohydrate intake at a specific time k, denoted as $\hat{CHO}(k)$ [g], is assumed to be consumed over a fixed interval D_{ut}. Thus, the rate of orally ingested carbohydrates is defined by the sequence $\hat{r}(k) = \{\hat{\mathbf{r}}_i\}_{i=0}^{N-1}$, where $\hat{r}_i = \frac{\hat{CHO}(k)}{D_{ut}}$ [g/min] for $i \in [0, n)$, and $\hat{r}_i = 0$ for $i \in [n, N-1]$, with $n = \frac{D_{ut}}{T_s} < N-1$ representing the meal duration in terms of sampling times, and N denoting the MPC control horizon. The same logic applies to the PA intensity, measured as the percentage of maximum oxygen consumption per minute [$\%VO_2^{max}$]. The intensity is spread over a duration D_{pt}, with the sequence defined by $\hat{p}(k) = \{\hat{\mathbf{p}}_i\}_{i=0}^{N-1}$, where $\hat{p}_i = \frac{\hat{PA}(k)}{D_{pt}}$ for $i \in [0, m)$, and $\hat{p}_i = 0$ for $i \in [m, N-1]$, with $m = \frac{D_{pt}}{T_s} < N-1$ representing the PA duration in terms of sampling times.

Thus, the cost function to be minimized by the MPC is given by:

$$\begin{aligned} &V_N(\hat{x}, \hat{\mathbf{r}}, \hat{\mathbf{p}}, \mathcal{Y}^{Tar}; \mathbf{u}, u_a, y_a, \boldsymbol{\delta_{hyper}}, \boldsymbol{\delta_{hypo}}, \delta_{hyper,s}, \delta_{hypo,s}) \\ &\quad \doteq V_{dyn}(\hat{x}, \hat{\mathbf{r}}, \hat{\mathbf{p}}; \mathbf{u}, u_a, y_a, \boldsymbol{\delta_{hyper}}, \boldsymbol{\delta_{hypo}}) \\ &\quad + V_s(\mathcal{Y}^{Tar}; u_a, y_a, \delta_{hyper,s}, \delta_{hypo,s}), \end{aligned} \tag{6}$$

where

$$\begin{aligned} &V_{dyn}(\hat{x}, \hat{\mathbf{r}}, \hat{\mathbf{p}}; \mathbf{u}, u_a, y_a, \delta_{hyper}, \delta_{hypo}) \\ &\quad \doteq \sum_{j=0}^{N-1} \|\delta_{hyper}(j)\|_{\hat{Q}}^2 + \|\delta_{hypo}(j)\|_{\hat{Q}}^2 + \|u(j) - u_a\|_R^2 \end{aligned}$$

is the dynamic cost term, aiming to steer the system toward the artificial equilibrium variables (u_a, y_a) through the predicted transient phase, with the equilibrium reached at the end of the control horizon N. Moreover:

$$V_s(\mathcal{Y}^{Tar}; u_a, y_a, \delta_{hyper,s}, \delta_{hypo,s}) \doteq \hat{\rho}\delta_{hyper,s}^2 + \check{\rho}\delta_{hypo,s}^2$$

is the stationary cost term that guides y_a towards the target equilibrium set $\mathcal{Y}^{Tar}$.

In contrast to the formulation presented in Licini et al. (2024), the pZMPC has been extended following the proposals presented in Abuin et al. (2024). In this formulation, $\mathbf{u} = \{u(0), u(1), \ldots, u(N-1)\}$ is the sequence of future control actions, while $\boldsymbol{\delta_{hyper}} = \{\delta_{hyper}(0), \delta_{hyper}(1), \ldots, \delta_{hyper}(N-1)\}$ and $\boldsymbol{\delta_{hypo}} = \{\delta_{hypo}(0), \delta_{hypo}(1), \ldots, \delta_{hypo}(N-1)\}$ are the sequences of deviation variables associated with hyperglycemia and hypoglycemia excursions, respectively. These sequences, along with the control actions, are the optimization variables. The slack variables $\delta_{hypo}(j)$ and $\delta_{hyper}(j)$, $j \in \mathbb{I}_{0:N-1}$, which are constrained to be positive, are weighted through matrices $\check{Q} \gg \hat{Q} > 0$. This last condition imposes asymmetry in the cost function, meaning the penalty for hypoglycemia is significantly higher than that for hyperglycemia, as the former presents a greater short-term risk (Gondhalekar et al., 2018). In this way, the predicted trajectory converges to y_a from above, decreasing hypoglycemic excursions with respect to the artificial set-point over the prediction horizon. Moreover, the stationary cost function penalizes the convergence of the system differently to the artificial equilibrium (u_a, y_a), by selecting $\check{\rho} \gg \hat{\rho}$. In this way, the convergence to the zone is more strongly promoted when y_a approaches $\mathcal{Y}$ from below. Finally, $R > 0$ represents the input weighting matrix, which is scalar in this case.

Then, the MPC optimization problem to be solved at each time k is formulated as follows:

$$\min_{\substack{\mathbf{u}, u_a, y_a, \\ \boldsymbol{\delta_{hyper}}, \boldsymbol{\delta_{hypo}}, \\ \delta_{hyper,s}, \delta_{hypo,s}}} V_N\left(\begin{array}{l} \hat{x}, \hat{\mathbf{r}}, \hat{\mathbf{p}}, \mathcal{Y}^{\mathrm{Tar}}; \\ \mathbf{u}, u_a, y_a, \boldsymbol{\delta}_{\mathrm{hyper}}, \boldsymbol{\delta}_{\mathrm{hypo}}, \delta_{\mathrm{hyper},s}, \delta_{\mathrm{hypo},s} \end{array} \right)$$

subject to:

$$x(0) = \hat{x}(k), \tag{7a}$$

$$x(j+1) = A^d x(j) + B_u^d u(j) + B_r^d r(j) + E^d, \quad j \in \mathbb{I}_{0:N-1}, \tag{7b}$$

$$u(j) \in \mathcal{U}, \quad j \in \mathbb{I}_{0:N-1}, \tag{7c}$$

$$\tilde{C}x(j) \in \tilde{C}\mathcal{X}(j; k), \quad j \in \mathbb{I}_{1:N}, \tag{7d}$$

$$\tilde{C}x(N) = x_a, \tag{7e}$$

$$x_a = \tilde{C}A^d x_a + \tilde{C}B^d u_a + \tilde{C}E^d, \tag{7f}$$

$$u_a \in \mathcal{U}, \tag{7g}$$

$$y_a = x_{1,a}, \tag{7h}$$

$$-\delta_{hypo}(j) \le Cx(j) - y_a \le \delta_{hyper}(j), \quad j \in \mathbb{I}_{1:N}, \tag{7i}$$

$$\mathcal{Y}_{min}^{Tar} - \delta_{hypo,s} \le y_a \le \mathcal{Y}_{max}^{Tar} + \delta_{hyper,s}, \tag{7j}$$

$$\delta_{hypo}(j) \ge 0, \ \delta_{hyper}(j) \ge 0, \quad j \in \mathbb{I}_{1:N} \tag{7k}$$

$$\delta_{hypo,s} \ge 0, \ \delta_{hyper,s} \ge 0. \tag{7l}$$

Constraint (7a) initializes the predicted state trajectory with the current state estimate $\hat{x}(k)$ provided by the ODO state estimator. In the model (7b), only the first three states are controllable, so constraints are imposed on x_1, x_2, and x_3 through the matrix $\tilde{C} = [I_3 \ 0_{3\times 4}]$. The state constraint (7d) is a discretization set $\mathcal{X}(t)$ defined in Section 2: state x_1 is bounded in accordance with physiological BG limits to prevent both severe hypo- and hyperglycemic excursions throughout the overall prediction horizon. The insulin states x_2 and x_3 are constrained by the non-standard insulin-on-board (nsIOB) constraint, following the approach in Abuin et al. (2024). This constraint is dynamically updated at each sample-time k and propagated through the prediction horizon for each step $j \in \mathcal{I}_{0:N-1}$. When a meal-related event occurs at time k with estimated carbohydrate content $\hat{CHO}_0$, the upper bound is relaxed from its basal value $IOB_b = \theta_4 \cdot 2U_b$, to $IOB_b + IOB_{pp}(k_0 + j; k_0, \hat{CHO}_0)$, where IOB_{pp} is the time-varying postprandial component. The terminal constraint (7e) forces the states at the end of the control horizon N to reach the artificial equilibrium state $x_a = [x_{1,a}, x_{2,a}, x_{3,a}]' \in \mathbb{R}^3$ (Krupa et al., 2024). Constraints (7h)–(7i)–(7j)–(7k)(7l) links the output auxiliary variable y_a to the state auxiliary variable x_a and establish the relationship between y_a and the asymmetric deviation variables $\delta_{hypo}(j)$ and $\delta_{hyper}(j)$. Finally, insulin delivery is constrained by the physical limitations of the pumps (MiniMed, 2018), through (7c). Once the problem is solved, the control law is given by $\kappa_{MPC}(\hat{x}, \hat{\mathbf{r}}, \hat{\mathbf{p}}, \mathcal{Y}^{Tar}) = u_0(0; x)$, where $u_0(0; x)$ is the first element of the solution sequence $\mathbf{u}^0$, following the application of a receding horizon control policy (RHC).

4. Simulation results

The proposed pZMPC was tested through in-silico simulations using a cohort of 10 adult patients from the FDA-approved UVA/Padova simulator for research (Group, 2016). The controller was implemented in MATLAB using the YALMIP toolbox for optimization (Lofberg, 2004).

4.1. Description of scenarios

The simulations covered 14 days, incorporating three nominal meals per day (60 g at 07:00, 60 g at 12:00, and 80 g at 18:00), subject to random variations in meal timing (±10 min) and meal size (±20%). Meals lasted 30 min for breakfast and lunch, and 40 min for dinner (±10 min). Physical activity was incorporated into the simulator following the strategy proposed in Schiavon et al. (2013). Exercise sessions followed two distinct schedules. The first scenario featured 45-minute sessions structured as follows: a 10-minute warm-up at light intensity (25% VO_{2max}), 10 min of high intensity (65% VO_{2max}), 20 min of moderate intensity (50% VO_{2max}), and a concluding 5-minute

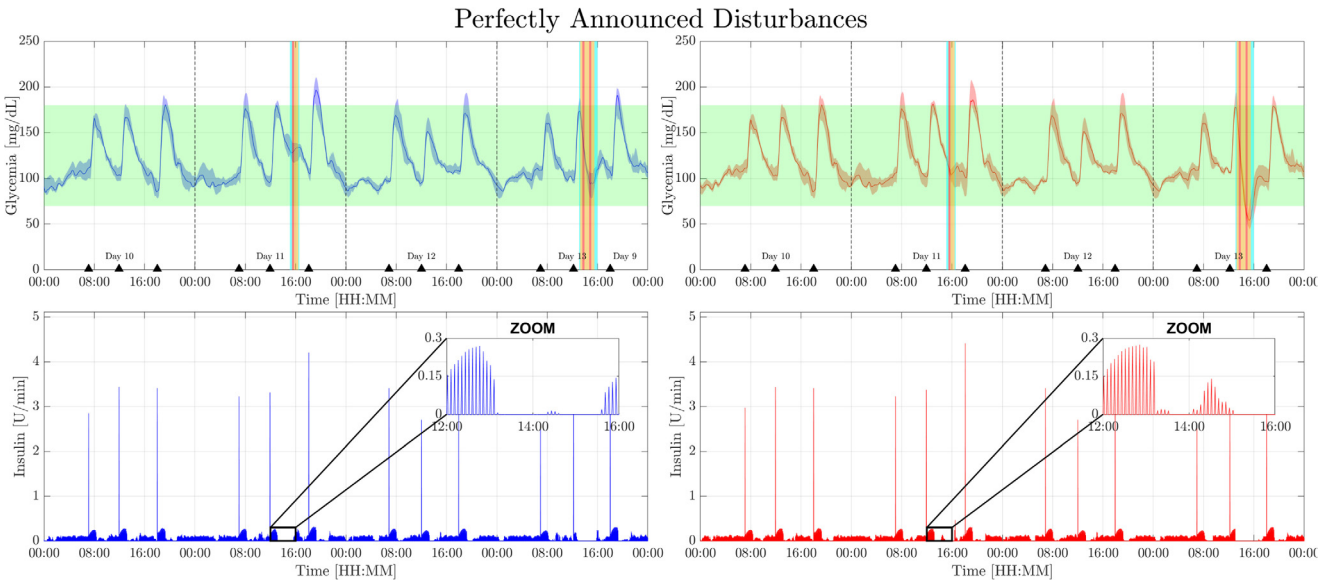

Fig. 2. Glycemic control under perfectly announced disturbances comparing programmed physical activity (left/blue) versus non-programmed approach (right/red). Top panels show median glucose trajectories (solid lines) with 25th–75th percentile ranges (shaded areas) and the target zone (green band). Black triangles indicate meal times. Bottom panels display insulin delivery patterns with zoomed sections before exercise events (colored vertical lines). When PA is programmed, insulin pulses are deliberately interrupted before exercise onset to reduce IOB; in the non-programmed case, the controller only reacts at activity onset and therefore does not preemptively suspend pulses. Post-activity small pulses can reappear when the MPC prediction indicates a modest insulin requirement to return glycemia to the target zone. These resumed microboluses occur within the IOB and glycemia safety bounds and are therefore consistent with safe operation.

cooldown at light intensity. The second scenario emulated a 90-minute session, thus simulating a longer workout. The schedule consisted of 5 min of light intensity, 10 min of moderate intensity, 10 min of high intensity, 25 min of moderate intensity, 10 min of high intensity, 15 min of moderate intensity, and 15 min of light intensity. Sessions were scheduled between 06:00 and 22:00, always at least 45 min post-meal, and alternated with rest days following ADA recommendations (Colberg et al., 2016). Similar to meals, PA intensity levels and individual phase durations (light, moderate, intense) varied by ±20%, and the entire workout schedule could shift by ±10 min.

The glucose sensor model used corresponds to Dexcom G5 Mobile CGM proposed in Vettoretti et al. (2018). The insulin pump was the default one provided by the simulator. Insulin delivery was administered exclusively through pulses, covering both basal and bolus insulin, each lasting $\Delta T_s = 1$ minute. The sampling time was set to T_s = 5 [min]. The MPC tuning parameters were chosen similarly to Abuin et al. (2024). Specifically, the stage cost matrices were configured as $\hat{Q} = 1$, $\check{Q} = 10^2$, and $R = 1$. The penalty weights for hyperglycemia and hypoglycemia deviations were set to $\hat{\rho} = 10^6$ and $\check{\rho} = 10^9$, respectively. The control horizon was fixed at 6 h ($N = 72$), in alignment with the ADA recommendations (American Diabetes Association, 2018). This tuning was applied uniformly across the entire cohort, with the exception of Adult 7, for whom a higher value of $\check{Q} = 10^3$ was used to account for the subject's higher mean insulin sensitivity.

Furthermore, the controller was designed for two different exercise scenarios: (i) Programmed PA, where the patient informs the AP in advance about their exercise sessions, and (ii) Non-Programmed PA, where the patient only notifies the AP at the onset of the exercise session. In the first case, the MPC includes the full feedforward information of the PA events throughout the entire prediction horizon, enabling it to optimize insulin delivery accordingly. This approach allows the MPC to anticipate the metabolic impacts of the PA events and adjust control actions to effectively manage glucose levels. In the second case, both CHO intake and PA characteristics (duration and intensity) are treated as disturbances announced only at their onset. We remark that this simulates an idealized instantaneous detection at exercise start; practical sensors or detection algorithms may introduce nonzero latency, which is noted below as a limitation. Both scenarios were thoroughly tested under increasingly complex conditions, including scenarios with inaccuracies in event announcements and circadian variations in insulin sensitivity (Toffanin et al., 2013), to robustly evaluate and validate the controller's performance.

4.2. Evaluation metrics

All performance indicators were calculated over the entire simulation horizon for each virtual subject. Results were subsequently aggregated at the cohort level and reported as median together with interquartile range (25th–75th percentile). The set of metrics comprises the following quantities: mean glucose (Gm); glucose standard deviation (SD); coefficient of variation, defined as CV(%) $= 100 \cdot$ SD/Gm; percentage of time spent within the euglycemic range 70–180 mg/dL (T_{70-180}) and within the tighter range 70–140 mg/dL (T_{70-140}); percentage of time above 180 mg/dL and 250 mg/dL ($T_{>180}$ and $T_{>250}$, respectively); percentage of time below 70 mg/dL and 54 mg/dL ($T_{<70}$ and $T_{<54}$, respectively); and total daily insulin delivered (TDI) expressed in U/day.

4.3. Scenario 1: Perfectly announced disturbances

The perfectly announced disturbances scenario represents the ideal case in which patients provide complete information about both meals and physical activity events, allowing the controller to incorporate these disturbances throughout the prediction horizon. Fig. 2 illustrates the glycemic outcomes under these conditions, comparing a scenario with Programmed PA (left panel, blue) with a Non-Programmed PA (right panel, red). Both trajectories display the median glucose profile (solid line) with 25th–75th percentile bands (shaded regions). As can be seen, scheduled/programmed PA management results in superior glycemic control compared with the non-programmed scenario. When PA events (indicated by colored vertical lines of varying

Table 2
Outcome metrics with perfectly and erroneously announced disturbances.

	Perfectly Announced		Erroneously Announced	
	Programmed	Non Programmed	Programmed	Non Programmed
Mean Gm [mg/dL]	117.6 [116.0, 119.6]	115.8 [114.5, 119.0]	117.8 [115.6, 119.2]	115.9 [114.8, 118.4]
SD [mg/dL]	27.9 [21.9, 30.5]	29.6 [22.6, 32.1]	29.2 [22.2, 31.9]	30.0 [23.0, 32.2]
CV [%]	24.4 [19.4, 26.0]	26.0 [20.2, 27.6]	25.5 [19.7, 26.8]	26.4 [20.6, 27.8]
T_{70-140} [%]	78.9 [76.3, 83.0]	77.3 [75.5, 82.8]	78.4 [74.9, 82.8]	77.0 [75.1, 82.9]
T_{70-180} [%]	96.6 [93.0, 98.1]	94.7 [91.0, 97.0]	95.3 [92.2, 98.1]	94.6 [91.0, 97.0]
$T_{>180}$ [%]	2.5 [1.1, 5.7]	1.9 [1.0, 5.6]	3.1 [1.4, 6.1]	2.3 [1.1, 5.9]
$T_{>250}$ [%]	0.0 [0.0, 0.0]	0.0 [0.0, 0.0]	0.0 [0.0, 0.0]	0.0 [0.0, 0.0]
$T_{<70}$ [%]	1.0 [0.4, 1.4]	2.4 [1.5, 3.4]	1.6 [0.7, 1.9]	2.6 [1.6, 3.1]
$T_{<54}$ [%]	0.1 [0.0, 0.5]	1.2 [0.5, 1.6]	0.5 [0.3, 0.8]	1.4 [0.5, 1.6]
TDI [U/day]	42.4 [38.0, 52.8]	42.5 [38.2, 52.9]	42.4 [37.9, 52.9]	42.5 [38.2, 53.1]

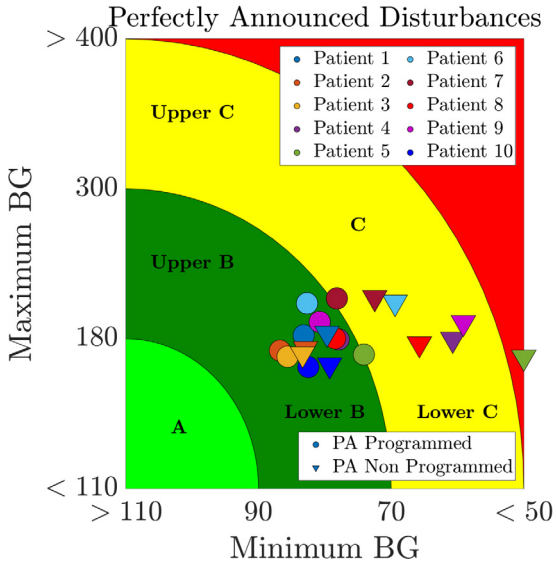

Fig. 3. CVGA results for perfectly announced disturbance conditions. The plot shows minimum (2.5th percentile) and maximum (97.5th percentile) blood glucose values for 10 virtual patients. Points represent individual patients, with distinction between programmed (circle) and non-programmed (triangle) physical activity scenarios. Colored zones indicate control quality: green (A) for optimal control, light green (B) for acceptable control, yellow (C) for suboptimal control, and red regions indicating potential hypo- or hyperglycemia.

intensities) are known in advance, the controller proactively modifies insulin delivery patterns. The bottom panels reveal this strategic approach, where insulin administration is deliberately interrupted before PA onset—creating a preemptive reduction in insulin-on-board that effectively prevents exercise-induced hypoglycemia while maintaining glucose levels within the target range despite meal and exercise challenges. In the non-programmed scenario, the controller reacts only at activity onset and therefore cannot preemptively suspend insulin delivery. Small insulin pulses may reappear after the PA period when the MPC prediction indicates a modest insulin requirement to return glycemia to the target zone. These resumed microboluses occur within the IOB and glycemia safety bounds (constraint (7d)) and are therefore consistent with safe operation: the asymmetric cost function strongly penalizes hypoglycemia, so the controller resumes pulses only when the predicted state and the non-standard IOB constraint allow additional insulin without violating G_{hypo}.

Quantitative results are reported in Table 2. The programmed approach shows better performance in several key metrics: both T_{70-180} [%] and T_{70-140} [%] are higher in the programmed approach, together with a lower glycemic variability (SD and CV), indicating improved overall control. The Control Variability Grid Analysis (CVGA) in Fig. 3 further quantifies these benefits by plotting the 2.5th and 97.5th percentiles of blood glucose values for each virtual patient. Circular markers, representing programmed PA scenarios, cluster predominantly in the desirable Lower B zone, indicating effective mitigation of both hyperglycemic and hypoglycemic extremes across the patient population. In contrast, the non-programmed scenario (triangular markers) exhibits a less favorable distribution, with markers located lower on the minimum BG axis (indicating greater hypoglycemia risk) and higher on the maximum BG axis (reflecting increased hyperglycemia severity).

4.4. Scenario 2: Erroneously announced disturbances

Uncertainty in patient-announced disturbances represents a critical challenge for AP systems, as real-world implementation inevitably faces imperfect meal and physical activity estimations. In this second scenario, the controller's robustness is evaluated under realistic conditions where patients imperfectly announce: (i) meals, by up ±50%, and (ii) exercise intensity by approximately ±20%. These announcement errors introduce a layer of variability that propagates through the control loop, resulting in a cascade of effects on glycemic regulation. Meal miscalculations particularly affect postprandial control. Underestimation leads to insufficient insulin delivery, causing persistent hyperglycemia, whereas overestimation increases the risk of hypoglycemic episodes, which can be especially dangerous when coinciding with physical activity. The asymmetric nature of these errors, where overestimated meals generally create more challenging control scenarios than underestimated ones, adds complexity to the control problem, as the single-hormonal system lacks positive control actions. Consequently, whereas a hyperglycemic condition can be mitigated by administering an additional insulin dose, the controllability of the system is significantly reduced in the case of hypoglycemia (or a tendency toward it). This scenario is further exacerbated when an overestimated meal coincides with an underestimated PA event Despite receiving erroneous information, the system maintains remarkable robustness, by showing only a minor degradation of 0.5% in the T_{70-140} [%] compared with the perfectly announced scenario (Table 2). The programmed approach still provided significant protection against hypoglycemia, with a $T_{<70}$ [%] of 1.6% (2.6% for the non-programmed approach). The expanded interquartile ranges visible in glucose trajectories of Fig. 4 directly reflect this announcement-induced variability, manifesting as wider glycemic excursions around median profiles compared to perfectly announced scenarios. Interpatient variability is magnified in these scenarios, with some patients maintaining reasonable control despite announcement errors, while others experience substantial deterioration. This reflects how identical announcement errors produce markedly different magnitudes of glycemic impact across individuals with a broad range of insulin sensitivities and glucose dynamics. Despite these multiple layers of variability (i.e., erroneously announced meal amount and

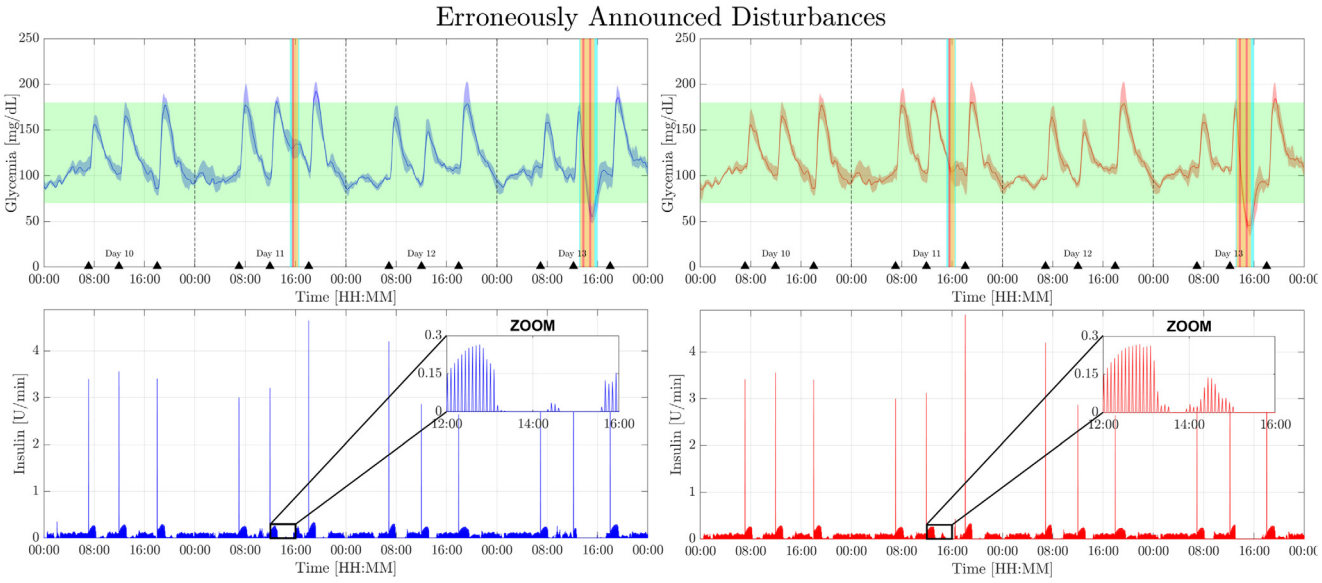

Fig. 4. Glycemic control under erroneously announced disturbances comparing programmed physical activity (left/blue) versus non-programmed approach (right/red). Top panels show median glucose trajectories (solid lines) with 25th-75th percentile ranges (shaded areas) and the target zone (green band). Bottom panels display insulin delivery patterns with zoomed sections highlighting strategic insulin interruption before exercise events (colored vertical lines). Black triangles indicate meal times.

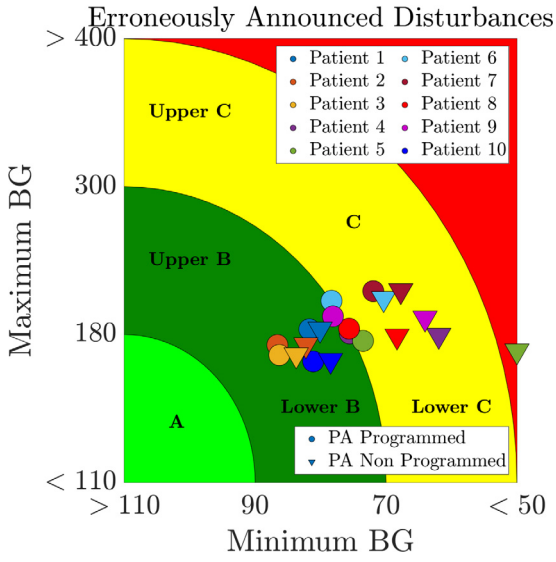

Fig. 5. CVGA results for erroneously announced disturbance conditions. The plot shows minimum (2.5th percentile) and maximum (97.5th percentile) blood glucose values for 10 virtual patients. Points represent individual patients, with distinction between programmed (circle) and non-programmed (triangle) physical activity scenarios. Colored zones indicate control quality: green (A) for optimal control, light green (B) for acceptable control, yellow (C) for suboptimal control, and red regions indicating potential hypo- or hyperglycemia.

physical activity intensity, and patient-specific blood glucose response) the controller maintains most patients within acceptable zones of glycemic control, (Fig. 5). In other words, this analysis reveals essential resilience for practical clinical application, where perfect disturbance announcements remain an unattainable ideal.

4.5. Scenario 3: Circadian variability

In this scenario, the AP system is challenged with physiological variations in insulin sensitivity that follow the circadian patterns described in Toffanin et al. (2013). This represents a more realistic testing environment as patients with T1DM experience natural fluctuations in insulin sensitivity throughout a 24-hour cycle (day- and nighttime periods).

Analysis of glycemic profiles over multiple days (Fig. 6) reveals similar patterns to the scenario without variability, highlighting the efficacy of programmed versus non-programmed control approaches. When disturbances, i.e., meals and activities, are perfectly announced (upper plots), the programmed approach maintains glucose predominantly within the TIR, effectively managing postprandial peaks and ensuring consistent glucose return to baseline between meals. Conversely, the non-programmed approach displays slightly higher postprandial peaks and greater variability, particularly noticeable overnight and early morning. Interestingly, when uncertainty in the announcements is present (Fig. 6, lower plots), the programmed approach demonstrates remarkable robustness. Despite uncertainties, glucose profiles closely resemble those seen with perfect announcements, and hypoglycemia risk is further reduced ($T_{<70}$ drops to 1.6%), suggesting that the controller adapts conservatively to uncertainty, providing additional safety margins. In contrast, the non-programmed approach remains less resilient, maintaining higher glycemic variability and consistent hypoglycemia risk ($T_{<70}$ of 2.7%). Statistical metrics reinforce these observations, with mean glucose consistently maintained across all scenarios (approximately 127–129 mg/dL). Glycemic variability indicators (standard deviation and coefficient of variation) show that the programmed approach consistently achieves lower variability, particularly under erroneous announcement conditions. Furthermore, T_{70-180} [%] is well maintained in all conditions, but notably optimal (86.2%) for the programmed approach under imperfect announcements. Some prandial glycemic peaks remain slightly elevated, especially those related to breakfast (i.e., the time of day when insulin sensitivity is lowest, at 40% of nominal, Toffanin et al. (2013)). The CVGA in Fig. 7 confirms the overall trend: all scenarios remain within acceptable zones, with the programmed approach consistently outperforming the non-programmed one.

5. Discussion

The results presented in Section 4 demonstrate that the proposed pZMPC framework effectively manages glucose regulation

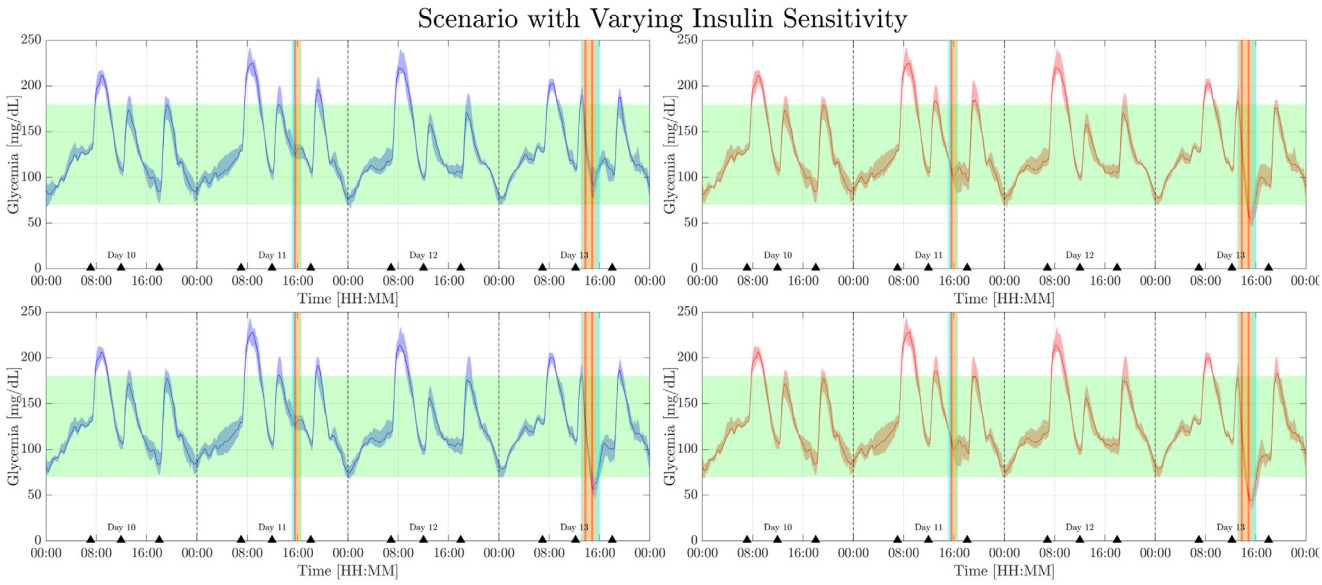

Fig. 6. Comparison of glycemic levels under circadian variability in insulin sensitivity, shown for both accurately announced disturbances (upper plots) and erroneously announced disturbances (lower plots).

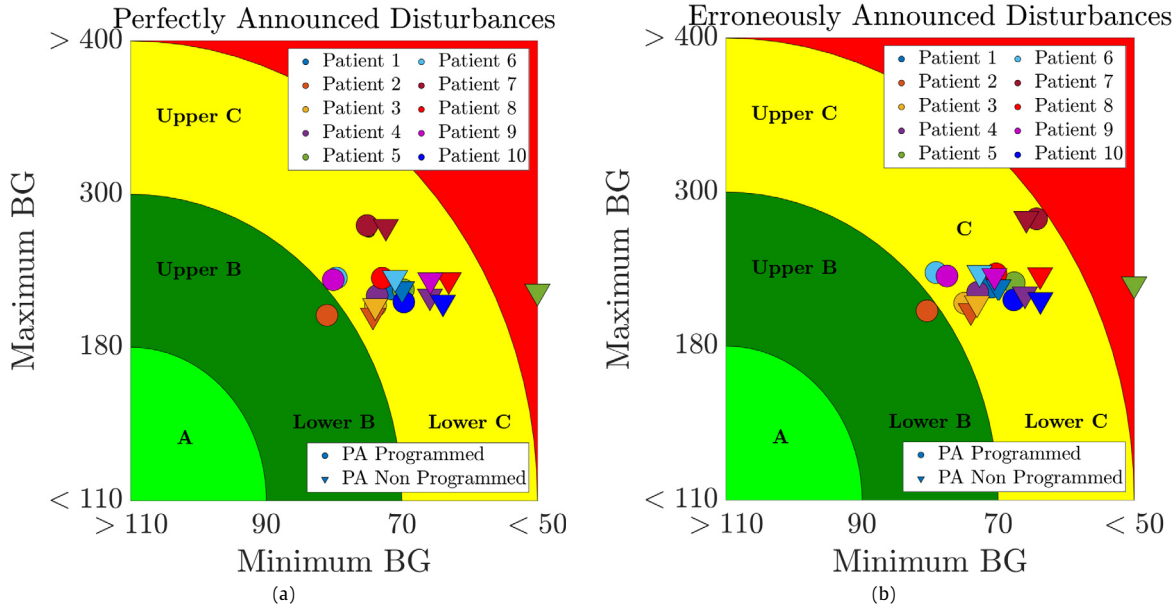

Fig. 7. CVGA results for both perfectly announced (left) and erroneously announced (right) disturbance conditions under circadian variability in insulin sensitivity.

across a range of realistic disturbance scenarios. In this section we discuss the key findings, and outline the limitations of the application.

5.1. Interpretation of key findings

The most significant performance gap between the programmed and non-programmed scenarios stems from the MPC ability to exploit its full 6-hour prediction horizon when the PA event is announced in advance. In the programmed condition, the feedforward PA profile is incorporated into the constrained optimization over the entire prediction horizon, allowing the controller to initiate insulin suspension well before exercise onset. This preemptive reduction in IOB is also a consequence of the non-standard IOB constraint interacting with the asymmetric cost function: since $\check{Q} \gg \hat{Q}$ and $\check{\rho} \gg \hat{\rho}$, the optimizer strongly favor approaching the target zone from above, naturally converging to a strategy that avoids hypoglycemia during exercise. In the non-programmed scenario, because the controller accounts for of the PA event only at its onset, no preemptive action is possible. The small insulin pulses that can appear shortly after the activity period (visible in Fig. 2, right panel) reflect the MPC solving problem in Section 3 with updated state information: once the elevated insulin-independent glucose uptake ($G_{PA}(t) = \theta_6 x_6(t)$) begins to subside after exercise, the predicted BG trajectory and the nsIOB constraint permit modest corrective pulses to steer the state back into the target zone $\mathcal{Y}^{Tar}$. The clearer and more prolonged insulin suspension during the second (longer, higher-intensity) exercise session is explained by the larger magnitude of the PA model term $G_{PA}(t)$: higher-intensity and longer-duration PA produces a stronger insulin-independent glucose uptake, prompting the MPC to extend the suspension to satisfy the IOB and G_{hypo} constraints.

Table 3
Outcome metrics when varying insulin sensitivity is considered.

	Perfectly Announced		Erroneously Announced	
	Programmed	Non Programmed	Programmed	Non Programmed
Mean Gm [mg/dL]	128.9 [124.1, 130.0]	127.1 [123.0, 129.1]	128.7 [124.3, 130.2]	127.0 [123.1, 129.1]
SD [mg/dL]	39.1 [34.8, 41.5]	39.6 [35.5, 42.6]	38.5 [34.3, 40.4]	39.3 [35.1, 41.7]
CV [%]	30.4 [28.1, 32.8]	31.0 [28.6, 33.7]	29.9 [27.6, 31.6]	30.9 [28.3, 33.2]
T_{70-140} [%]	69.2 [67.0, 72.2]	69.7 [67.0, 71.9]	69.8 [69.2, 72.6]	69.6 [67.5, 71.9]
T_{70-180} [%]	85.0 [83.6, 88.2]	84.1 [83.0, 87.5]	86.2 [84.2, 88.8]	84.2 [83.2, 87.7]
$T_{>180}$ [%]	12.2 [9.4, 14.7]	11.7 [9.4, 14.3]	11.7 [9.1, 14.2]	11.6 [9.2, 14.2]
$T_{>250}$ [%]	0.0 [0.0, 0.2]	0.0 [0.0, 0.2]	0.0 [0.0, 0.1]	0.0 [0.0, 0.1]
$T_{<70}$ [%]	2.2 [1.6, 2.9]	2.6 [2.3, 3.6]	1.6 [1.3, 2.1]	2.7 [2.1, 3.8]
$T_{<54}$ [%]	0.5 [0.3, 0.8]	1.1 [0.5, 1.5]	0.2 [0.0, 0.4]	1.0 [0.5, 1.4]
TDI [U/day]	44.6 [40.3, 55.4]	44.7 [40.6, 55.8]	44.6 [40.5, 55.3]	44.7 [40.8, 55.8]

For shorter or milder sessions the predicted BG recovers faster, and the MPC allows modest corrective pulses earlier. Thus, observed differences between sessions primarily reflect (i) the PA magnitude and duration encoded in the model states x_6, x_7, and (ii) the interaction with the nsIOB constraint and the asymmetric cost.

When announcement errors are introduced (Scenario 4.4), the variability challenge is compounded when PA errors overlap with meal announcement errors, creating a multi-dimensional uncertainty pattern that the controller must handle simultaneously. However, the zone-based formulation proves particularly valuable in managing this variability, prioritizing the maintenance of glucose within safe boundaries rather than precise tracking of reference values, which inherently provides tolerance to disturbance uncertainty.

Circadian variability (Scenario 4.5) substantially increases glycemic variability, as reflected by increased SD, CV, and $T_{>180}$, due to the reduced insulin sensitivity during early morning hours (40% of nominal). Despite this physiological challenge, the programmed approach consistently achieves the best outcomes, confirming the robustness of the pZMPC framework. Some residual prandial peaks at breakfast reflect the mismatch between the fixed controller tuning and the time-varying sensitivity; possible solutions could mitigate this limitation and are proposed as future work, such as the introduction of a velocity-weighting function as in Gondhalekar et al. (2018), or using multiple patient-specific models throughout the day (Toffanin et al., 2019).

To further characterize the distribution of hypoglycemic events[1] across the cohort, Table 4 complements the aggregate $T_{<70}$ and $T_{<54}$ reported in Tables 2–3 with per-patient counts of mild (N<70 mg/dL) and severe (N<54 mg/dL) hypoglycemic events. Mild events are consistently more frequent in the Non-Programmed configurations across all patients and under both insulin sensitivity conditions (see Table 4). For instance, under the Nominal IS, Perfectly Announced condition, the median number of mild events is 3 vs. 5 for the Programmed and Non-Programmed configurations. Severe events are absent in 3 out of 10 patients under the Perfectly Announced – Programmed – No Variability configuration (cohort median: 1.0 vs. 4.5 for Non Programmed), confirming the benefit of accurate PA programming under nominal IS conditions.

Under circadian variability, PA may occur during periods of near-nominal or elevated IS (Toffanin et al., 2019). In this context, the feedforward insulin suppression, calibrated on a constant θ_2, can become excessive when the actual IS exceeds the model assumption, potentially leading to severe hypoglycaemia in the post-exercise phase. However, an interesting trend can be observed: both the $T_{<54}$ metric (Tables 3) and the number of severe hypoglycaemic events for several patients (e.g., Patients 3, 4, 6, and 9) suggest that the Erroneously Announced – Programmed configuration is associated with fewer severe events compared to the Perfectly Announced – Programmed case. This apparently counterintuitive behavior can be explained by the interaction of multiple sources of mismatch under circadian IS variability. On the one hand, overestimation of PA intensity in the erroneous announcement leads to a stronger insulin reduction than required, which can unintentionally create a protective buffer against late post-exercise hypoglycaemia. On the other hand, the nsIOB constraint – computed assuming constant θ_2 – does not fully capture the variations in insulin action induced by circadian changes in IS. In this setting, the slightly lower overall insulin delivery observed in the erroneous case may interact more favorably with such mismatches. These mechanisms act jointly *only* under time-varying IS, which explains why the trend is absent in the No-Variability condition and is consistent with the asymmetric cost function design, which already penalizes hypoglycaemia more severely than hyperglycaemia.

5.2. Study limitations and future work

Several limitations of this study should be acknowledged, which remain for future research.

First, the PA model in (1) captures only the insulin-independent component of exercise-induced glucose clearance. Extending the embedded model to incorporate the insulin-dependent variation of PA sensitivity, following the proposal by Romeres et al. (2021), represents a natural and important next step.

Second, further validation of the proposed approach in a broad cohort, including both adolescents and children, is an essential next step toward practical implementation. Moreover, in this work, each virtual patient was simulated over a single 14-day period with randomized day-to-day variability in meal and PA timing and size.

Third, in the non-programmed scenario, the simulations assume instantaneous detection of PA at exercise onset (zero announcement delay). In practice, wearable sensors or patient-activated detection may introduce nonzero latency, which could reduce the controller's responsiveness and warrants further investigation in future studies.

Finally, inter-patient variability is evident across all scenarios and reflects the wide range of insulin sensitivities and glucose dynamics in the cohort. While the uniform tuning strategy (identical MPC parameters for all patients, except Adult 7) demonstrates the framework's generalizability, further personalization of control parameters remains an important avenue for improving outcomes across diverse patient populations.

[1] According to International Consensus on Use of Continuous Glucose Monitoring, an event is defined as glucose readings below the specified threshold for at least 15 min (Danne et al., 2017).

Table 4
Hypoglycemic event counts (N) per patient in all scenarios. Mild: N<70 mg/dL; Severe: N<54 mg/dL. Summary row: median [25th, 75th percentile] across the 10 virtual patients.

Patient		Nominal IS				Circadian IS			
		Perfectly Announced		Erroneously Announced		Perfectly Announced		Erroneously Announced	
		Programmed	Non-Programmed	Programmed	Non-Programmed	Programmed	Non-Programmed	Programmed	Non-Programmed
001	N<70	3	5	5	4	9	10	9	8
	N<54	0	1	1	2	0	2	2	2
002	N<70	3	5	2	5	4	7	3	7
	N<54	1	2	1	2	1	2	1	2
003	N<70	2	3	2	3	7	6	6	7
	N<54	0	0	1	1	0	1	1	1
004	N<70	4	6	4	6	5	5	4	5
	N<54	0	4	1	5	0	3	1	4
005	N<70	4	7	4	7	9	11	10	12
	N<54	2	6	2	6	2	5	2	5
006	N<70	4	6	5	6	4	6	4	6
	N<54	2	5	3	4	2	4	3	3
007	N<70	4	6	6	7	4	6	7	7
	N<54	3	4	5	5	3	4	7	6
008	N<70	2	7	5	7	8	12	8	10
	N<54	0	5	2	5	1	5	3	5
009	N<70	3	6	4	6	3	6	4	5
	N<54	2	6	2	4	2	5	2	3
010	N<70	1	5	2	5	9	13	10	12
	N<54	1	2	1	2	1	2	2	3
Median [25,75]	N<70	3.0 [2.0, 4.0]	6.0 [5.0, 6.0]	4.0 [2.0, 5.0]	6.0 [5.0, 7.0]	6.0 [4.0, 9.0]	6.5 [6.0, 11.0]	6.5 [4.0, 9.0]	7.0 [6.0, 10.0]
	N<54	1.0 [0.0, 2.0]	4.0 [2.0, 5.0]	1.5 [1.0, 2.0]	4.0 [2.0, 5.0]	1.0 [0.0, 2.0]	3.5 [2.0, 5.0]	2.0 [1.0, 3.0]	3.0 [2.0, 5.0]

6. Conclusion

This paper has presented a comprehensive model of glucose regulation in type 1 diabetes that explicitly integrates physical activity effects into an artificial pancreas system. The proposed pulsatile Zone Model Predictive Control (pZMPC) strategy demonstrates robust performance across challenging scenarios that reflect real-world conditions, including variable exercise intensities, announcement errors, and circadian variations in insulin sensitivity. The integration of physical activity into the control system architecture through a dedicated linear model proves particularly valuable in preventing exercise-induced hypoglycemia while maintaining effective overall glycemic control. Our results quantify the benefits of exercise announcement, showing that when the physical activity event is programmed (i.e., foreseen in advance over the prediction horizon), time-in-range increases and hypoglycemic events decrease compared to non-programmed scenarios. Moreover, due to the asymmetric cost function, the convergence to the target zone was promoted from hyperglycemic regions, providing an effective mechanism to balance the competing risks of hyper- and hypoglycemia, with a focus on preventing dangerous low-glycemic events during and after exercise. This effect is particularly visible in the variable insulin sensitivity scenario, where, despite the increment in time above the range, there was no significant rise in time below the range. Similarly, the incorporation of the non-standard IOB constraint improves the controller's ability to safely manage postprandial excursions despite meal announcement errors.

In conclusion, this work demonstrates that explicitly incorporating physical activity into the control framework represents a significant advancement toward fully automated glucose regulation in real-world scenarios. In particular, the MPC approach effectively leverages anticipated events, substantially improving performance while consistently reducing time spent in hypoglycemia, marking a meaningful step forward in addressing a key challenge of diabetes management.

CRediT authorship contribution statement

Nicola Licini: Writing – review & editing, Writing – original draft, Validation, Investigation, Formal analysis, Conceptualization. **Beatrice Sonzogni:** Supervision, Formal analysis, Conceptualization. **Pablo Abuin:** Supervision, Formal analysis, Conceptualization. **Fabio Previdi:** Supervision, Funding acquisition. **Alejandro H. González:** Supervision, Formal analysis, Conceptualization. **Antonio Ferramosca:** Supervision, Formal analysis, Conceptualization.

Declaration of competing interest

The authors declare that they have no known competing financial interests or personal relationships that could have appeared to influence the work reported in this paper.

Acknowledgments

This work was funded by the National Plan for NRRP Complementary Investments (PNC, established with the decree-law 6 May 2021, n. 59, converted by law n. 101 of 2021) in the call for the funding of research initiatives for technologies and innovative trajectories in the health and care sectors (Directorial Decree n. 931 of 06-06-2022) – project n. PNC0000003 – AdvaNced Technologies for Human-centrEd Medicine (project acronym: ANTHEM). This work reflects only the authors' views and opinions, neither the Ministry for University and Research nor the European Commission can be considered responsible for them - CUP B53C22006700001.

Appendix. Discrete time modeling for pulsatile input signals

To effectively implement the continuous-time model (1) within an MPC framework, the model must first be discretized through sampling. The common method used is the zero-order hold (ZOH) assumption, which relies on a continuous and constant infusion delivery $u(t)$ $[U/min]$ over the time interval between samples. However, as detailed in Brazeau et al. (2013) and Roversi et al. (2020), better BG control can be achieved by

accounting for short-duration insulin actions, represented by a pulsatile model.

Building on the insights from Abuin et al. (2020), a pulsatile injection scheme is reasonable since insulin pumps typically deliver insulin via microboluses over the sampling period (Song et al., 2000). Thus, the pulsatile input scheme proposed in Abuin et al. (2020) and Licini et al. (2024) is employed. Given a sampling time T_s, the input $u(t)$ is defined as follows:

$$u(t) = \begin{cases} u(kT_s), & t \in [kT_s, kT_s + \Delta T_s), \\ 0, & t \in [kT_s + \Delta T_s, (k+1)T_s), \end{cases}$$

for $k \in \mathbb{I}_{[0,\infty)}$, where $\Delta \in (0, 1]$ represents the pulse duration. The disturbances $r(t)$ and $p(t)$ are sampled as $r(t) = r(kT_s)$ and $p(t) = p(kT_s)$ over the interval $t \in [kT_s, (k+1)T_s), k \in \mathbb{N}_{\geq 0}$, following the typical ZOH assumption.

Sampling the continuous-time solution at times $t = kT_s$, the discrete-time system becomes:

$$\begin{aligned} x((k+1)T_s) =& A^d x(kT_s) + B_u^d u(kT_s) \\ &+ B_r^d r(kT_s) + B_p^d p(kT_s) + E^d, \end{aligned}$$

where the matrices A^d, B_r^d, B_p^d, and E^d are the discrete-time counterparts of A, B_r, B_p, and E for the period T_s. The matrix B_u^d reflects the insulin effect, which is zero from ΔT_s to T_s due to the pulsatile input behavior. These matrices are computed as follows:

$$\begin{aligned} &A^d = e^{AT_s}, \quad B_u^d = e^{A(T_s - \Delta T_s)} A^{-1}(e^{A\Delta T_s} - I_7)B_u, \\ &B_r^d = A^{-1}(e^{AT_s} - I_7)B_r, \quad B_p^d = A^{-1}(e^{AT_s} - I_7)B_p, \\ &E^d = A^{-1}(e^{AT_s} - I_7)E. \end{aligned}$$

Remark 4. Pulsatile systems require careful handling when characterizing equilibria due to the control-free response period from ΔT_s to T_s (as defined in Abuin et al. (2020)). For simplicity, we assume control equilibria are characterized by pairs (u_s, x_s) satisfying $x_s = A^d x_s + B^d u_s + E^d$. Due to the pulsatile inputs, these equilibria differ from the continuous-time control equilibria.

References

Abuin, P., Ferramosca, A., Toffanin, C., Magni, L., & González, A. H. (2024). Pulsatile Zone MPC with asymmetric stationary cost for artificial pancreas based on a non-standard IOB constraint. *Journal of Process Control*, *136*, Article 103191. http://dx.doi.org/10.1016/j.jprocont.2024.103191.

Abuin, P., Rivadeneira, P., Ferramosca, A., & González, A. (2020). Artificial pancreas under stable pulsatile MPC: Improving the closed-loop performance. *Journal of Process Control*, *92*, 246–260. http://dx.doi.org/10.1016/j.jprocont.2020.06.009.

American Diabetes Association (2003). Physical Activity/Exercise and Diabetes Mellitus. *Diabetes Care*, *26*(suppl_1), s73–s77. http://dx.doi.org/10.2337/diacare.26.2007.S73.

American Diabetes Association (2018). 6. Glycemic Targets: Standards of Medical Care in Diabetes—2019. *Diabetes Care*, *42*(Supplement_1), S61–S70. http://dx.doi.org/10.2337/dc19-S006.

Bondia, J., Romero-Vivo, S., Ricarte, B., & Diez, J. L. (2018). Insulin Estimation and Prediction: A Review of the Estimation and Prediction of Subcutaneous Insulin Pharmacokinetics in Closed-Loop Glucose Control. *IEEE Control Systems*, *38*(1), 47–66. http://dx.doi.org/10.1109/MCS.2017.2766312.

Brazeau, A., Mircescu, H., Desjardins, K., Leroux, C., Strychar, I., Ekoé, J., & Rabasa-Lhoret, R. (2013). Carbohydrate counting accuracy and blood glucose variability in adults with type 1 diabetes. *Diabetes Research and Clinical Practice*, *99*(1), 19–23. http://dx.doi.org/10.1016/j.diabres.2012.10.024.

Colberg, S. R., Sigal, R. J., Yardley, J. E., Riddell, M. C., Dunstan, D. W., Dempsey, P. C., Horton, E. S., Castorino, K., & Tate, D. F. (2016). Physical Activity/Exercise and Diabetes: A Position Statement of the American Diabetes Association. *Diabetes Care*, *39*(11), 2065–2079. http://dx.doi.org/10.2337/dc16-1728.

Dalla Man, C., Breton, M. D., & Cobelli, C. (2009). Physical Activity into the Meal Glucose—Insulin Model of Type 1 Diabetes: *In Silico* Studies. *Journal of Diabetes Science and Technology*, *3*(1), 56–67. http://dx.doi.org/10.1177/193229680900300107.

Danne, T., Nimri, R., Battelino, T., Bergenstal, R. M., Close, K. L., DeVries, J. H., Garg, S., Heinemann, L., Hirsch, I., Amiel, S. A., Beck, R., Bosi, E., Buckingham, B., Cobelli, C., Dassau, E., Doyle, F. J., Heller, S., Hovorka, R., Jia, W., ... Phillip, M. (2017). International Consensus on Use of Continuous Glucose Monitoring. *Diabetes Care*, *40*(12), 1631–1640. http://dx.doi.org/10.2337/dc17-1600.

Gondhalekar, R., Dassau, E., & Doyle, F. J. (2018). Velocity-weighting & velocity-penalty MPC of an artificial pancreas: Improved safety & performance. *Automatica*, *91*, 105–117. http://dx.doi.org/10.1016/j.automatica.2018.01.025.

Group, T. E. (2016). DMMS.R, T. E. group.

Howorka, K. (2012). *Functional Insulin Treatment: Principles, Teaching Approach and Practice*. Springer Science & Business Media.

Incremona, G. P., Messori, M., Toffanin, C., Cobelli, C., & Magni, L. (2018). Model predictive control with integral action for artificial pancreas. *Control Engineering Practice*, *77*, 86–94. http://dx.doi.org/10.1016/j.conengprac.2018.05.006.

Katsarou, A., Gudbjörnsdottir, S., Rawshani, A., Dabelea, D., Bonifacio, E., Anderson, B. J., Jacobsen, L. M., Schatz, D. A., & Lernmark, A. (2017). Type 1 diabetes mellitus. *Nature Reviews Disease Primers*, *3*(1), 17016. http://dx.doi.org/10.1038/nrdp.2017.16.

Krupa, P., Köhler, J., Ferramosca, A., Alvarado, I., Zeilinger, M., Alamo, T., & Limon, D. (2024). Model predictive control for tracking using artificial references: Fundamentals, recent results and practical implementation. In *2024 IEEE 63rd conference on decision and control* (pp. 2977–2991). Milan, Italy: IEEE, http://dx.doi.org/10.1109/CDC56724.2024.10886854.

Licini, N., Sonzogni, B., Abuin, P., Previdi, F., Gonzalez, A. H., & Ferramosca, A. (2024). Artificial Pancreas under stable pulsatile Model Predictive Control: Including the Physical Activity effect. In *2024 IEEE 63rd conference on decision and control* (pp. 4028–4033). Milan, Italy: IEEE, http://dx.doi.org/10.1109/CDC56724.2024.10886334.

Lofberg, J. (2004). YALMIP : A toolbox for modeling and optimization in MATLAB. In *2004 IEEE international conference on robotics and automation (IEEE cat. no.04CH37508)* (pp. 284–289). http://dx.doi.org/10.1109/CACSD.2004.1393890, 0002/2004-09-04.

Mansell, E. J., Docherty, P. D., & Chase, J. G. (2017). Shedding light on grey noise in diabetes modelling. *Biomedical Signal Processing and Control*, *31*, 16–30. http://dx.doi.org/10.1016/j.bspc.2016.06.007.

MiniMed, M. (2018). MINIMED™ 670G SYSTEM USER GUIDE. *Medtronic MiniMed*.

Riddell, M. C., Gallen, I. W., Smart, C. E., Taplin, C. E., Adolfsson, P., Lumb, A. N., Kowalski, A., Rabasa-Lhoret, R., McCrimmon, R. J., Hume, C., Annan, F., Fournier, P. A., Graham, C., Bode, B., Galassetti, P., Jones, T. W., Millán, I. S., Heise, T., Peters, A. L., ... Laffel, L. M. (2017). Exercise management in type 1 diabetes: A consensus statement. *The Lancet Diabetes & Endocrinology*, *5*(5), 377–390. http://dx.doi.org/10.1016/S2213-8587(17)30014-1.

Romeres, D., Schiavon, M., Basu, A., Cobelli, C., Basu, R., & Dalla Man, C. (2021). Exercise effect on insulin-dependent and insulin-independent glucose utilization in healthy individuals and individuals with type 1 diabetes: A modeling study. *American Journal of Physiology-Endocrinology and Metabolism*, *321*(1), E122–E129. http://dx.doi.org/10.1152/ajpendo.00084.2021.

Roversi, C., Vettoretti, M., Del Favero, S., Facchinetti, A., & Sparacino, G. (2020). Modeling Carbohydrate Counting Error in Type 1 Diabetes Management. *Diabetes Technology & Therapeutics*, *22*(10), 749–759. http://dx.doi.org/10.1089/dia.2019.0502.

Roy, A. (2007). Dynamic Modeling of Exercise Effects on Plasma Glucose and Insulin Levels. *1*, (3).

Ruan, Y., Wilinska, M. E., Thabit, H., & Hovorka, R. (2017). Modeling Day-to-Day Variability of Glucose–Insulin Regulation Over 12-Week Home Use of Closed-Loop Insulin Delivery. *IEEE Transactions on Biomedical Engineering*, *64*(6), 1412–1419. http://dx.doi.org/10.1109/TBME.2016.2590498.

Schiavon, M., Man, C. D., Kudva, Y. C., Basu, A., & Cobelli, C. (2013). *In Silico* Optimization of Basal Insulin Infusion Rate during Exercise: Implication for Artificial Pancreas. *Journal of Diabetes Science and Technology*, *7*(6), 1461–1469. http://dx.doi.org/10.1177/193229681300700606.

Song, S. H., Mcintyre, S. S., Shah, H., Veldhuis, J. D., Hayes, P. C., & Butler, P. C. (2000). Direct Measurement of Pulsatile Insulin Secretion from the Portal Vein in Human Subjects. *85*, (12).

Toffanin, C., Aiello, E., Del Favero, S., Cobelli, C., & Magni, L. (2019). Multiple models for artificial pancreas predictions identified from free-living condition data: A proof of concept study. *Journal of Process Control*, *77*, 29–37. http://dx.doi.org/10.1016/j.jprocont.2019.03.007.

Toffanin, C., Zisser, H., Doyle, F. J., & Dassau, E. (2013). Dynamic Insulin on Board: Incorporation of Circadian Insulin Sensitivity Variation. *Journal of Diabetes Science and Technology*, *7*(4), 928–940. http://dx.doi.org/10.1177/193229681300700415.

Vettoretti, M., Facchinetti, A., Sparacino, G., & Cobelli, C. (2018). Type-1 Diabetes Patient Decision Simulator for In Silico Testing Safety and Effectiveness of Insulin Treatments. *IEEE Transactions on Biomedical Engineering*, *65*(6), 1281–1290. http://dx.doi.org/10.1109/TBME.2017.2746340.